

Hybrid Camera Pose Estimation with Online Partitioning

Xinyi Li Haibin Ling
 Department of Computer Science
 College of Science and Technology
 Temple University
 {xinyi.li, haibin.ling}@temple.edu

Abstract

This paper presents a hybrid real-time camera pose estimation framework with a novel partitioning scheme and introduces motion averaging to on-line monocular systems. Breaking through the limitations of fixed-size temporal partitioning in most conventional pose estimation mechanisms, the proposed approach significantly improves the accuracy of local bundle adjustment by gathering spatially-strongly-connected cameras into each block. With the dynamic initialization using intermediate computation values, our proposed self-adaptive Levenberg-Marquardt solver achieves a quadratic convergence rate to further enhance the efficiency of the local optimization. Moreover, the dense data association between blocks by virtue of our co-visibility-based partitioning enables us to explore and implement motion averaging to efficiently align the blocks globally, updating camera motion estimations on-the-fly. Experiment results on benchmarks convincingly demonstrate the practicality and robustness of our proposed approach by outperforming conventional bundle adjustment by orders of magnitude.

1. Introduction

1.1. Background

With low-cost hand-held scanning devices made widely available in recent years, simultaneous localization and mapping (SLAM) and structure-from-motion (SfM) systems have been extensively studied during the past decades. Camera pose estimation, lying at the core of most feature-based multi-view geometry systems, aims to jointly refine the coordinates of 3D landmarks and camera parameters along the camera trajectory. As a robot scans surrounding scenes, the photometric information is transitioned into geometric correspondences which then serve as the constraints in solving a non-linear least squares system.

Comprehensive existing approaches have been proposed to address the camera motion estimation problem. Consid-

ered as the arguably most popular approach, *bundle adjustment* (BA) has received extensive research attention. For instance, *incremental BA* ([19,26,34,36,38,42]) starts by initializing the map reconstruction with few images and later measurements are incrementally merged with iterative essential matrix updates. Many state-of-the-art SLAM systems ([18,20,23]) implement incremental BA to compromise speed and accuracy. However, incremental approaches are well-observed to be prone to accumulated drifting errors and sensitive to poor initialization, resulting in the deteriorated performance progressively over long camera trajectories. Alternatively, *hierarchical BA* ([5,16,29,32,35,37]) pre-clusters the images and then solves the smaller sub-problems separately. Though achieving excellent results for the off-line SfM problem, hierarchical approaches require global view-graph information in advance such that the applicability for generalized real-time systems is hindered. Many other challenging issues of BA remain open, *e.g.*, the cubic-order complexity with regards to the number of image frames involves prohibitive computational costs [42]; slow or erroneous convergences of the numerical solvers due to the intrinsically high dimensional solution space, *etc.* To tackle the aforementioned issues, this paper presents a hybrid pose estimation framework combining BA and *motion averaging* for on-line monocular systems.

With the efficient implementations of motion averaging ([3,4,7,12,15,46,47]), promising results have recently been shown in distributed SfM frameworks ([6–8,45–47]). [46] proposes a camera clustering algorithm and presents a hybrid pipeline applying the parallel-processed local increment into global motion averaging framework. In [47], a divide-and-conquer framework is introduced to address distributed large-scale motion averaging problems and shows convincing results on city-scale datasets. Inspired by the superior performances, we propose a *quasi-distributed* formulation and introduce *single rotation averaging* into real-time pose estimation tasks.

Previous works most related to ours include [5], [27] and [2], among which [5] and [27] both aim to solve the

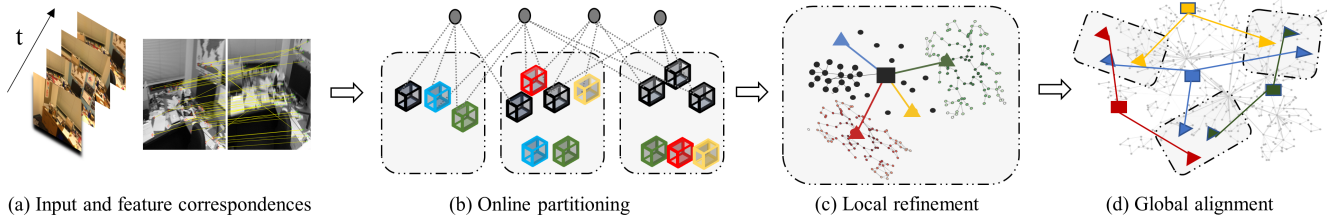


Figure 1: The pipeline of our proposed algorithm: (a) the input image sequence and feature correspondence, (b) the on-line partitioning based on local and global co-visibility (§3.1), (c) the refinement of local pose-graph with semi-distributed initialization (§3.2), (d) the progressive global alignment by motion averaging with common camera parameters (§3.3).

off-line SfM problem. In [5], the authors propose a unified framework where global rotation averaging is implemented in a community-based manner, followed by local incremental BA for individual camera refinement. Relaxing the requirement in [5] of prior global knowledge for the complete view graph, [27] is capable of processing both unordered and sequential data. However, it is impractical to directly apply [27] to on-line systems since 1) the progressive brute-force image matching for the clustering struggles to deliver real-time performance; and 2) the global multiple similarity averaging based on exhaustively dense inter-cluster connections reaches the memory and computation limits of real-time systems very soon. [2] presents a motivating BA-free SLAM framework where only camera orientations are estimated and maintained via rotation averaging. However, global optimality of the camera parameters in the proposed framework is not claimed and the accuracy compared with state-of-the-art systems is not provided.

To the best of our knowledge, our approach is the first hybrid framework combining BA and motion averaging to estimate and update the camera poses on-the-fly.

1.2. Our Contributions

In this paper, we propose a novel hybrid formulation to solve the real-time camera pose estimation problem in a quasi-distributed manner. In order to break through the limitations of fixed-size partitioning in the conventional framework, we instead partition cameras into blocks based on both temporal and spatial co-visibility. Specifically, in addition to temporally-adjacent cameras, each block contains cameras added from previous blocks if sufficient overlapping views are detected between the cameras and the current block.

The local optimization process in conventional BA refines the camera poses within sequential partitions of fixed sizes, and frequently suffers from slow or erroneous convergences due to noisy data. By contrast, our partitioning scheme gathers spatially-strongly-connected intra-block cameras to improve the accuracy of the local optimization afterwards. Our proposed partitioning scheme also encourages the propagation of intermediate computation values

between blocks which later benefits the local BA in a two-fold aspect: 1) good initialization is dynamically provided; and 2) duplicate computations are effectively avoided. The satisfying initialization also sheds light on our proposed self-adaptive Levenberg-Marquardt solver, which achieves a quadratic convergence rate and thus further enhances the local BA efficiency.

Shared camera parameters among different blocks, produced by our partitioning scheme, allow us to close the gaps between off-line and on-line systems and introduce motion averaging into solving real-time pose estimation tasks. By leveraging single rotation averaging on the common camera parameters in multiple blocks, we effectively reduce drifting errors while tackling the computational bottleneck of conventional formulation of global BA. Moreover, by virtue of the dense connectivity between blocks based on global co-visibility, our approach can skip explicit loop closing to further accelerate the global alignment.

As shown in the experiments, our approach clearly outperforms state-of-the-art conventional BA-based systems in both efficiency and accuracy. Experimental results on large-scale outdoor scene dataset further demonstrates the robustness of our proposed framework.

In summary, the key contributions of our paper are:

- We develop a novel hybrid real-time camera pose estimation framework with co-visibility-based partitioning scheme designed for online monocular systems.
- We introduce motion averaging to efficiently update the camera poses on-the-fly, conquering the computational bottleneck of conventional global BA and avoiding explicit loop closing.
- With the dynamic inter-block propagation and intra-block broadcasting of intermediate computation values, we introduce a generic self-adaptive Levenberg-Marquardt solver achieving a quadratic convergence rate and analyze the convergence conditions.

The rest of the paper is organized as follows. A brief review of BA and motion averaging is given in §2. We then introduce the proposed approach in §3, followed in §4 by the description of our self-adaptive Levenberg-Marquardt

solver. At last, we report the experimental results in §5, and draw conclusions in §6.

2. Preliminaries and Notations

Bundle adjustment (BA) is a fundamental technique in SLAM and SfM systems. By minimizing the sum of re-projection errors for given observations of the 3D scene, BA iteratively refines camera/pose parameters and 3D point coordinates simultaneously.

Consider a given 3D scene with m image frames and n observable 3D points. Let $p_i^j \in \mathbb{R}^2$ denote the observation coordinate of 3D point $P_j \in \mathbb{R}^3$ on image frame I_i for $1 \leq i \leq m, 1 \leq j \leq n$. We define the projection mapping $\pi(K, C_i, P_j) : \mathcal{K} \times \mathcal{C} \times \mathbb{R}^3 \mapsto \mathbb{R}^2$, where $K \in \mathcal{K} \subseteq \mathbb{R}^3$ denotes the camera intrinsic matrix and is considered known and fixed for a calibrated system throughout the paper; $C_i = [R_i | t_i] \in \mathcal{C} \subseteq \mathbb{SE}(3) \subseteq \mathbb{R}^{3 \times 4}$ denotes the absolute camera pose of I_i , where the rotation part is denoted by $R_i \in \mathbb{SO}(3) \subseteq \mathbb{R}^{3 \times 3}$ and the translation part is denoted by $t_i \in \mathbb{R}^3$. The re-projection error minimization is thus defined as

$$\min_{\substack{C_i \in \mathcal{C}, 1 \leq i \leq m \\ P_j, 1 \leq j \leq n}} \sum_{i=1}^m \sum_{j=1}^n \mathbb{I}_{ij} \|p_i^j - \pi(K, C_i, P_j)\|_2^2, \quad (1)$$

where \mathbb{I} denotes the visibility matrix, *i.e.*, $\mathbb{I}_{ij} = 1$ if P_j is visible on I_i and 0 otherwise. In §3.2 we describe the local optimization process by solving sub-problems of Eq. 1.

Motion averaging, as an alternative approach, aims to optimize the camera motion based on several known camera orientations. In this paper we leverage the *single rotation averaging* to align the camera blocks globally, where single rotations are computed given multiple measurements by the process of averaging. Formally, let $R_{ii'}$ denote the relative rotation from I_i to $I_{i'}$, *i.e.* $R_{ii'} = R_{i'} R_i^\top$, we define the objective function of optimization as

$$\arg \min_{R_{ii'} \in \mathbb{SO}(3)} \sum_{k \in \mathbb{N}} d(\widetilde{R_{ii'}^k}, R_{ii'})^2, \quad (2)$$

where $\widetilde{R_{ii'}^k} \in \mathbb{SO}(3)$ denotes the estimation of $R_{ii'}$ by the k^{th} observation; $d(\cdot, \cdot)$ denotes the proper metric, in this paper we use the Kacher mean, *i.e.*, the geodesic L_2 -mean for the computation. Formally, define the metric $d(X, Y) = d_{\mathcal{L}}(XY^\top, I) = \|\log(XY^\top)\|_2, \forall X, Y \in \mathbb{SO}(3)$. Further implementation details are illustrated in §3.3.

3. The Hybrid Formulation

In this section, the details of our hybrid pose estimation formulation are described. We propose to dynamically partition the cameras into blocks according to both temporal and spatial co-visibility, producing blocks of spatially-strongly-connected cameras (§3.1). Since we allow the

same cameras to appear ubiquitously, the corresponding parameters can thus be quasi-distributedly optimized within different blocks in the local optimization afterwards (§3.2). In order to efficiently initialize the iterations of local BA, we also propagate the intermediate computation values of the common camera parameters from previous blocks into the current block broadcasting in a greedy manner. Once local BA is finished for one block, the intra-block relative motions are considered fixed and single rotation averaging is then performed on the shared camera parameters among blocks in the global alignment (§3.3).

3.1. Online Partitioning

Key to our proposed algorithm is to timely partition the incoming sequence into blocks where cameras within the same block are spatially-strongly-connected regarding co-visible 3D scene points. Precisely, we enforce that most 3D points are visible by a sufficient amount of cameras to ensure the intra-block camera-camera connectivity. Besides, we allow the cameras from previous sequential blocks to be added into the current block if sufficient camera-block overlapping views are detected.

Given the input sequence of m image frames, each frame I_i is parameterized by $\{C_i, \mathbf{P}_i\}$ with $\mathbf{P}_i = \{P_j | \mathbb{I}_{ij} \neq 0\}$ as the set of visible 3D points on I_i . We aim to partition the sequence into m_b blocks $\mathcal{B}^l = \{\mathcal{C}^l, \mathcal{P}^l\}, 1 \leq l \leq m_b$, assuming m^l cameras are partitioned into \mathcal{B}^l , then $\mathcal{C}^l = \{C_i^l \in \mathcal{C}\}_{i=1}^{m^l}$ denotes the set of cameras and $\mathcal{P}^l = \cup_{i=1}^{m^l} \mathbf{P}_i$ denotes the union set of 3D points visible by the entire \mathcal{C}^l . Since we encourage cameras to appear in multiple blocks, the blocks produced by our partitioning scheme satisfy the following

$$\begin{aligned} \cup_{l=1}^{m_b} \mathcal{C}^l &= \cup_{i=1}^m C_i, \cup_{l=1}^{m_b} \mathcal{P}^l = \cup_{i=1}^m \mathbf{P}_i, \\ \exists 1 \leq l' \neq l \leq m_b \text{ s.t. } &\mathcal{C}^l \cap \mathcal{C}^{l'} \neq \emptyset, \end{aligned} \quad (3)$$

i.e. for each block, there exists at least one block such that the two blocks have common cameras. In details, our proposed partitioning criterion consists of two parts as described in the following discussions, namely, the *local co-visibility* and the *global co-visibility*.

The local co-visibility is defined as the average degree of connectivity between the cameras within a block. Specifically, the accuracy of the intra-block BA can be asserted with each single 3D point visible by a sufficient number of cameras. However, it is implausible to employ this principle in real-time applications since it can introduce a large number of redundant cameras. Alternatively, we define the *local co-visibility score* γ^l for \mathcal{B}^l by averaging the camera numbers over the 3D point set, and use it to guide the block construction. Formally, let \mathbf{p}_j^l denote the union set of projected 2D points on all in-block camera frames from a 3D

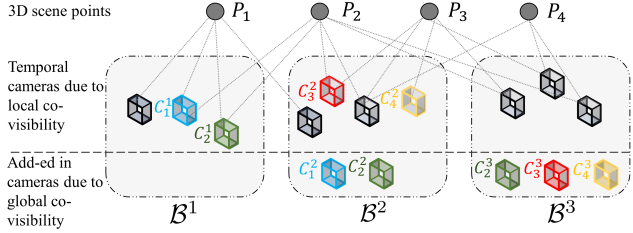


Figure 2: Our online partitioning scheme partitions the cameras into blocks based on both temporal and spatial co-visibility. Core of our algorithm is that one camera can be optimized within different blocks (e.g. C_1 is estimated in \mathcal{B}^1 and \mathcal{B}^2 , marked as C_1^1 and C_1^2 , respectively) as long as the camera shares sufficient overlapping views with the blocks.

point $P_j \in \mathcal{P}^l$, then

$$\gamma^l = \sum_{j=1}^{|\mathcal{P}^l|} \frac{|\mathbf{p}_j^l|}{|\mathcal{P}^l|}, \quad (4)$$

where $|\cdot|$ denotes the size of a set. We require that $\gamma^l \geq \gamma^{\text{thr}}$, where $\gamma^{\text{thr}} \geq 3$ is a preset parameter that determines the average size of the blocks, e.g., with a higher value of γ^{thr} , blocks with greater sizes are expected. By enforcing a minimum local average co-visibility, the accuracy of local BA inside each block is improved with sufficiently many point-camera constraints. New image frames are sequentially partitioned into current block \mathcal{B}^l while $\gamma^l < \gamma^{\text{thr}}$, we therefore limit the size of each block by n^{thr} in order to keep each block small for the real-time performance. Note that for scenarios where the camera is moving fast in feature-less scenes, our approach degrades to the conventional fixed-size partitioning. Once the local co-visibility score meets the criterion, block is temporally fixed followed by the add-in's of the image frames satisfying the global co-visibility requirement as illustrated below.

The global co-visibility is defined as the degree of camera-block connectivity, i.e., instead of only optimizing the frames in the current temporal block, cameras with sufficient overlapping views from previous blocks are added into the current block. The *global co-visibility score* β_i^l for the co-visibility between the current block \mathcal{B}^l and a previous image frame I_i (i.e., $C_i \in \mathcal{C}^{l'}, l' < l$) is defined as

$$\beta_i^l = \frac{|\mathbf{P}_i \cap \mathcal{P}^l|}{|\mathcal{P}^l|}. \quad (5)$$

I_i can thus be added into \mathcal{B}^l if $\beta_i^l > \beta^{\text{thr}}$, where $\beta^{\text{thr}} \in [0, 1)$ is a preset parameter defining the minimum camera-block overlapping view ratio. Furthermore, we set an *upper bound* n_α for the added-in cameras, which is particularly important when the capturing density is considerably high (e.g. camera moving around small-scale scenes for a long duration), as the high volume of overlapping visible regions

can introduce an excessive amount of cameras therefore causing noisy data and additional computations. In practice, higher values of γ^{thr} , n_α and n^{thr} combined with a lower global co-visibility threshold β^{thr} achieve a better accuracy with trade-offs of a slower convergence and higher computational cost. In our experiments we choose $\gamma^{\text{thr}} = 10$, $\beta^{\text{thr}} = 0.15$, $n_\alpha = 10$ and $n^{\text{thr}} = 50$ to balance between accuracy and efficiency. We illustrate our partitioning scheme in Fig. 2.

Note that two consecutive blocks share *at least one* overlapping frame: the last temporal frame in the previous block is the first temporal frame in the current block by default. The current block is considered fixed at the completion of adding cameras from previous blocks, hence proceeding to the following local optimization.

3.2. Local Optimization

We first reformulate Eq. 1 into the sub-problem for \mathcal{B}^l , the objective function of the local optimization is defined as

$$(\mathcal{C}^l, \mathcal{P}^l)^* = \arg \min_{\substack{C_i \in \mathcal{C}^{m_l}, P_j \in \mathbb{R}^{3 \times n_l} \\ C_i \in \mathcal{C}^l \\ P_j \in \mathcal{P}^l}} \sum_{C_i \in \mathcal{C}^l} \sum_{P_j \in \mathcal{P}^l} \mathbb{I}_{ij} \|P_i^j - \pi(K, C_i, P_j)\|_2^2. \quad (6)$$

To iteratively solve Eq. 6 we follow the Levenberg-Marquardt algorithm [25], which is well-known to be sensitive to the initialization. Indeed, conventional BA often suffers from converging to the local minima when the starting point is poorly chosen. By virtue of our partitioning scheme, we tackle the initialization issue by propagating the intermediate computation values of the parameters of added-in cameras from previous blocks.

In details, the added-in cameras carry computation values from the previous intra-block local BA, we can thus initialize the local BA iterations of the current block with the intermediate results. Hence the local optimization of each block can quasi-distributedly launch as soon as the block is fixed, with no delay on requesting final computation results of previous block. Additionally, we broadcast the intermediate values based on the intra-block camera connectivity in a greedy manner.

Formally, let $\mathcal{G}^l = \{\mathcal{V}^l, \mathcal{E}^l\}$ denote the intra-block pose-graph for \mathcal{B}^l , where the vertices in \mathcal{V}^l represent the cameras and the edges in \mathcal{E}^l are defined by the co-visibility between two image frames, i.e.,

$$\mathcal{V}^l = \{C_i | C_i \in \mathcal{C}^l\}, \quad (7a)$$

$$\mathcal{E}^l = \{e_{ij} | 1 \leq i \leq m_l, 1 \leq j \leq n_l\}, \quad (7b)$$

where $e_{ij} = 1$ if there exists co-visible 3D points between frames I_i and I_j and 0 otherwise. The broadcasting of the parameters is conducted by generating a Maximum Spanning Forest (MSF) of multiple Maximum Spanning Trees (MST) [24] from \mathcal{G}^l as discussed below.

Let \mathcal{C}_α^l denote the set of cameras added into \mathcal{B}^l from previous blocks, where $\mathcal{C}_\alpha^l = \{C_\alpha^i | 1 \leq i \leq n_\alpha\}$. Each C_α^i in the set is initialized as the root of a MST \mathcal{T}_i^l , and we initialize the weights in such a way that the weight w_{ij} between the roots C_α^i and the non-root vertices C_j are the co-visibility counts ($\geq cov^{thr}$) and 0 otherwise. Formally,

$$w_{ij} = \mathcal{X}_{\geq cov^{thr}} |\mathbf{P}_\alpha^i \cap \mathbf{P}_j|, 1 \leq \forall j \neq i \leq m_l, \quad (8)$$

where $\mathcal{X}_{\geq cov^{thr}}$ denotes the corresponding indicator function. We follow [33] to obtain the updated pose-graph $\mathcal{G}^{l'} = \{\mathcal{V}^{l'}, \mathcal{E}^{l'}\}$ where $\mathcal{V}^{l'} \subseteq \mathcal{V}^l$. The camera parameters are then initialized with those of the corresponding roots.

Note that $\mathcal{T}_i^{l'}$'s can possibly contain only a subset of the vertices \mathcal{V}^l since there might be intra-block cameras which share no common viewpoints with those in \mathcal{C}_α^l . Poses of these cameras are therefore initialized with the reference frame of the block. We define the first frame of each block (as is also the last frame of the previous block) as the *local reference frame* of \mathcal{B}^l , i.e., $I_r^l \triangleq I_1^l$.

So far we have obtained the MSF \mathcal{M}^l from \mathcal{G}^l with disjoint $\mathcal{T}_i^{l'}$'s properly defined, formally, $\mathcal{M}^l = \{\mathcal{T}_i^l | i = 1, \dots, n_\alpha\} \cup \mathcal{T}_r^l$. Based on the observation that camera motions are likely to be bounded within a small range given the local co-visibility condition defined in §3.1, we argue that our initialization mechanism feeds the local BA with initial values sufficiently close to the optimal solution. We can then adopt our proposed *self-adaptive Levenberg-Marquardt solver* (§4.1) on solving Eq. 6 for the set of camera poses relative to C_r^l . The intra-block relative poses are fixed upon the termination of local BA and the block is globally aligned with peer blocks in the consequent stage.

3.3. Global Alignment

As the results of each local BA are provided, we are now ready to align the blocks progressively to ensure the global consistency. Blocks are densely connected by multiple camera parameters by virtue of our partitioning scheme, allowing us to uncover more accurate inter-block transformations compared with single-keyframe-based conventional global BA. Moreover, in order to tackle the computational bottleneck of global optimization based on point-camera correspondences, we leverage single motion averaging on the camera parameters shared in different blocks.

Once the local optimization is finished for a block, all the previous blocks which share common camera parameters with the current block are globally aligned. Specifically, several estimations of the same camera pose are derived from different blocks such that we can exploit Eq. 2 to measure the inter-block relative motions. Consider that two blocks $\mathcal{B}^l = \{\mathcal{C}^l, \mathcal{P}^l\}$ and $\mathcal{B}^{l'} = \{\mathcal{C}^{l'}, \mathcal{P}^{l'}\}$ share a common set ${}^l_l \mathcal{C}$ of camera parameters, where ${}^l_l \mathcal{C} = \mathcal{C}^l \cap \mathcal{C}^{l'}$. Denote \widetilde{C}_i^l and $\widetilde{C}_i^{l'}$ for the camera poses relative to the correspond-

ing reference frames C_r^l and $C_r^{l'}$, we thus have

$${}^l_l \widetilde{\mathcal{C}} = \{\widetilde{C}_i^l, \widetilde{C}_i^{l'} | l \neq l'; i = 1, \dots, |{}^l_l \mathcal{C}|\}, \quad (9a)$$

$${}^l_l \widetilde{\mathcal{R}} = \{\widetilde{R}_i^l, \widetilde{R}_i^{l'} | l \neq l'; i = 1, \dots, |{}^l_l \mathcal{C}|\}, \quad (9b)$$

where ${}^l_l \widetilde{\mathcal{R}}$ denotes the set of measurements of relative rotations. We further define the inter-block relative rotation, as we aim to solve in the global alignment, $R_{ll'} = R_{l'} R_l^\top$ from \mathcal{B}^l to $\mathcal{B}^{l'}$, where R_l and $R_{l'}$ are the *pseudo* absolute rotations of the corresponding reference frames, note that we never require the absolute rotation parameters in our algorithm. It thus follows that, the estimated relative rotation $\widetilde{R}_{ll'}$ can be represented as follows

$$\widetilde{R}_{ll'} = \left(\widetilde{R}_i R_{l'}^\top \right)^\top \left(\widetilde{R}_i R_l^\top \right) = \widetilde{R}_i^{\top} \widetilde{R}_i^l. \quad (10)$$

Then we can solve the inter-block relative rotation $R_{ll'}$ by rewriting Eq. 2 into the following form,

$$\arg \min_{R_{ll'} \in \mathbb{SO}(3)} \sum_{i=1}^{|{}^l_l \mathcal{C}|} d\left(\widetilde{R}_{ll'}^i, R_{ll'}\right)^2. \quad (11)$$

We are now ready to generalize Eq. 11 into the global optimization with all of the blocks where the local optimizations have been finished with the updated relative motion parameters. To find the set of aligned rotations \mathcal{R}_{m_b} for m_b blocks, where $\mathcal{R}_{m_b} = \{R_{jj'} | 1 \leq j \neq j' \leq m_b\}$, we minimize the global rotation estimation error by solving

$$\arg \min_{R_{jj'} \in \mathbb{SO}(3)} \sum_{j \neq j'}^{m_b} \sum_{i=1}^{|{}^j_j \mathcal{C}|} d\left(\widetilde{R}_{jj'}^i, R_{jj'}\right)^2. \quad (12)$$

We argue that $d_\perp(\widetilde{R}_{jj'}^i, R_{jj'}) \in [0, \pi], \forall i, j, j'$ to guarantee the global convergence and follow the algorithm in [30] for the optimization. In practice, the global alignment runs in parallel with the local optimization once a block is ready and Eq. 12 is iteratively optimized only with the latest rotation parameters of the common cameras.

Compared with conventional global BA based on point-camera correspondences, our algorithm can achieve a much lower computational complexity and almost constant runtime with increasing number of image frames. For on-line systems where input image frames are sequentially processed, the inter-block global co-visibility stays on a stable level. Fig. 3a shows that the total re-projection error increases in a much lower rate compared to incremental and keyframe-based hierarchical BA. In Fig. 3b it can be observed that our global alignment is constantly 60-150x faster than that of conventional global BA based on point-camera correspondences. Moreover, according to the detection of the camera-block overlapping views based on global co-visibility, our algorithm can skip explicit loop closings to further accelerate the global alignment.

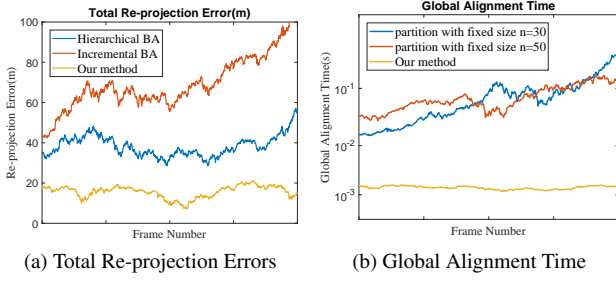


Figure 3: Comparison with conventional global BA on the accuracy and runtime. (a) shows the accumulated re-projection error comparison with conventional hierarchical BA and incremental BA methods. (b) shows the run-time comparison with conventional keyframe-based global BA with fixed-size partitions. The experiments are conducted on Seq.02 of KITTI Odometry [13].

4. Self-Adaptive Numerical Solver

4.1. Self-adaptive Iterations

To efficiently solve local optimization problem defined in §3.2 with the intermediate results propagated from other blocks as the initial values, we propose a modified Levenberg-Marquardt solver assuming a initialization sufficiently close to the optimal solution set. Precisely, the step size of the iteration is updated according to the size of the block, achieving a quadratic convergence rate.

Letting $f(x) \equiv [f_1(x), \dots, f_m(x)]$ denote the stacked vector of re-projection errors where $f_i(x)$ represent the re-projection error on image frame I_i , to solve Eq. 6 we consider the equivalent non-linear system

$$f(x) = 0, \text{ s.t. } x \in \Omega, \quad (13)$$

where f is continuously differentiable. Let \mathcal{H} denote a Hilbert space, then $\Omega \subseteq \mathcal{H} \subseteq \mathbb{R}^{6m} \otimes \mathbb{R}^{3n}$ denotes the assumingly non-emepty solution set. We further define the related optimization problem

$$\min_{x \in \mathcal{H}} \phi(x), \text{ with } \phi : \mathcal{H} \mapsto \mathbb{R} \text{ given by } \phi(x) = \|f(x)\|_2^2. \quad (14)$$

Let $\nabla f(x)$ denote the approximation to the *matrix gradient* (the transpose of the Jacobian matrix $J(x)$) of f at x , i.e. $\nabla f(x) = J^\top(x)$. Then the Levenberg-Marquardt method is conventionally implemented to solve Eq. 14 by iteratively generating a sequence of convex sub-problems

$$\min_{d \in \mathcal{H}} \psi_k(d), \text{ with } \psi_k : \mathcal{H} \mapsto \mathbb{R} \text{ given by} \quad (15a)$$

$$\psi_k(d) = \|\nabla f(x_k)^\top d + f(x_k)\|_2^2 + \mu_k \|d\|_2^2, \quad (15b)$$

$$(\nabla f(x_k) \nabla f(x_k)^\top + \mu_k I) d_k = -\nabla f(x_k) f(x_k), \quad (15c)$$

where d in Eq. 15b is solved to compute the direction d_k in Eq. 15c, $I \in \mathcal{H} \otimes \mathcal{H}$ denotes the identity matrix. $\mu_k \in \mathbb{R}$, namely Levenberg-Marquardt parameter, is updated with adaption to properly handle the cases where

$\nabla f(x_k) \nabla f(x_k)^\top$ is singular. The Levenberg-Marquardt method is well-proven to achieve a quadratic convergence rate to a solution x^* of Eq. 13 if $\nabla f(x^*)$ is nonsingular, where the nonsingularity also implies that the solution to Eq. 14 must be locally unique. However, the assumption of nonsingularity fails for the conventional BA problems.

Motivated by [43], we assume a much weaker assumption, namely, *local error bound condition* than the nonsingularity of $\nabla f(x^*)$. Denote $\text{dist}(y, \Omega) = \inf_{x \in \Omega} \|y - x\|_2$, recall the local error bound condition as

$$\exists \delta, \beta > 0 \text{ s.t. } \beta \text{dist}(x, \Omega) \leq \|f(x)\|_2, \quad \forall x \in B_\delta(x^*) \cap \Omega, \quad (16)$$

where $B_\delta(x^*) = \{x \in \mathcal{H} | \text{dist}(x, x^*) \leq \delta\}$.

Given that the Eq. 16 holds, the choice of Levenberg-Marquardt parameter μ_k plays a key role in the Levenberg-Marquardt convergence. We argue that the initialization of the iteration sequence defined in Eq. 6 is sufficiently close to the solution set Ω by propagating and broadcasting the common camera parameters as illustrated in §3.2. Letting $\mu_k = \alpha_k \|f(x_k)\|_2^\lambda$ in Eq. 15b thus leads to the quadratic rates of local convergence for Eq. 14, where α_k is iteratively updated to control the *trust region* radius of searching a satisfactory d_k . In details,

$$\mu_k = \alpha_k \|f(x_k)\|_2^\lambda, \quad (17a)$$

$$\Phi_k = \phi(x_k) - \phi(x_k + d_k), \quad (17b)$$

$$\Psi_k = \phi(x_k) - \min_{d_k \in \mathcal{H}} \|\nabla f(x_k)^\top d_k + f(x_k)\|_2^2, \quad (17c)$$

where Φ_k and Ψ_k can be considered as the actual and predicted reduction for the merit function, respectively. The parameter $\nu_k \in (0, 1)$ is introduced to the iterative system in order to serve as an indicator of whether the current d_k benefits towards the solution, further guiding the update rule of α_k . Formally,

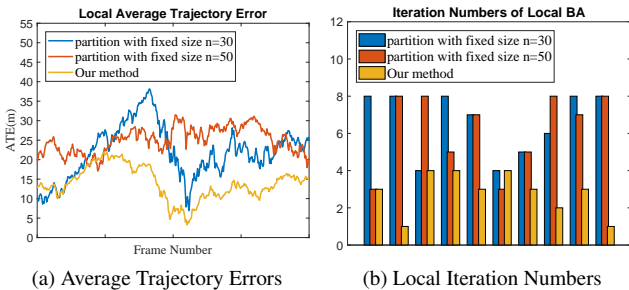
$$\nu_k = \frac{\Phi_k}{\Psi_k}, \quad (18a)$$

$$\alpha_{k+1} = \rho(\eta, \alpha_k, \nu_k; \nu), \quad (18b)$$

where $\nu \in (0, 1)$ is a given constant, $\eta > 1$ is a positive integer, $\rho(\eta, \alpha, \nu; \nu) : \mathbb{N}_{>0} \times \mathbb{R} \times (0, 1) \mapsto \mathbb{R}_{\geq 0}$ is continuous and nonnegative (here we let $\rho(\eta, \alpha, \nu; \nu)$ be strictly positive by enforcing a sufficiently small lower bound $\xi > 0$), defined as

$$\rho(\eta, \alpha_k, \nu_k; \nu) = \alpha_k \max\{\xi, 1 - \eta^{\lceil \frac{1}{\nu} \rceil} (\nu_k - \nu)^{2^{\lceil \log_2 \eta \rceil - 1}}\}. \quad (19)$$

Our formulation of Eq. 19 can be seen as a variant of the update rule in [9] and [17], the proposed iteration scheme has the following desirable properties: (i) $\nu_k = \nu$ is the only inflection point, i.e. $\frac{\partial^2 \rho}{\partial \nu_k^2} < 0$ if $\nu_k < \nu$ and the opposite holds otherwise; (ii) $\rho_\nu(\eta, \alpha_k, \nu_k) > \alpha_k \forall \eta, \alpha_k$, if $\nu_k < \nu$ and the opposite holds otherwise. Specifically, the properties imply that as $\nu_k < \nu$ and gets smaller (e.g. close to 0), α_k (and thus μ_k) are enlarged at a higher rate to improve the searching for a better d_k ; for the contrary case



(a) Average Trajectory Errors (b) Local Iteration Numbers

Figure 4: Comparisons with conventional BA with fixed-size partitions. (a) shows the average trajectory errors for the local block with the peaks representing that a new block is being processed. (b) shows the iterations required for the convergence of the intra-block local BA. The experiments are conducted on Seq.02 of KITTI Odometry [13].

when ν_k is close to 1, α_k can be legitimately reduced since d_k is satisfactory. In addition, we let $\eta = m_l$ for the problem defined in Eq. 6 with m_l image frames. Since a high value of n foresees a slow convergence, we thus add the power term $(2\lceil \log_2 \eta \rceil - 1)$ such that the sensitivity of ρ_ν with regards to ν_k increases with adaption for a greater n to preserve the convergence speed for large-scale problems. The convergence properties is shown similar to [9, 10, 21] in the supplementary materials.

4.2. Convergence Improvement

The local pose refinement is conducted in an incremental BA manner with our proposed Levenberg-Marquardt solver. Our algorithm improves the local optimization in two-fold: First, with our local co-visibility threshold defined for the partitioning scheme, it is guaranteed that a majority of the 3D points are observable by a sufficient amount of cameras to provide the high accuracy. Second, the inter-block propagation of the intermediate computational values greatly benefits the convergence of local Levenberg-Marquardt iterations, by providing the close-to-optimal initialization.

We compare our proposed approach on local convergence accuracy and local iteration numbers with conventional BA with fixed-size partitions by regular Levenberg-Marquardt solver. The comparisons are provided in Fig. 4. While partition with bigger size ($n = 50$) provides slightly higher accuracy, it typically requires more iterations till the local convergence. Our method requires significantly fewer iterations while producing comparable or better accuracy. More details on convergence properties are provided in supplementary materials.

5. Experimental Results

5.1. Implementation Details

System Configuration All of our experiment results are achieved from a PC with Intel(R) i7-7700 3.6GHz proces-

	DVO SLAM [22]	Kintinuous [39]	Elastic Fusion [40]	ORB SLAM [31]	ENFT SFM [44]	Visual SFM [41]	OURS
fr1_desk	2.1	3.7	2.0	1.7	2.7	2.7	1.6
fr1_desk2	4.6	7.1	4.8	2.9*	3.6*	-	1.5
fr1_room	4.3	7.5	6.8	3.4*	5.3*	-	2.9
fr2_desk	1.7	3.4	7.1	0.8	2.3	1.7	1.5
fr2_xyz	1.8	2.9	1.1	0.3	0.8	0.7	0.3
fr3_office	3.5	3.0	1.7	3.5	1.2	1.1	0.8
fr3_nst_near	1.8	3.1	1.6	1.4	1.9	1.1	1.1

Table 1: Trajectory estimation RMSE (cm) on the TUM RGB-D [14] dataset. Results with (*) are experimental results based on 5-execution medians from running open-source codes provided by the authors. The first three systems are using depth data while our results are based on RGB data only.

sors, 8 threads and 64GB memory.

Methods and Datasets We compare our proposed method with several state-of-the-art SLAM systems including: DVO-SLAM [22], Kintinuous [39], Elastic Fusion [40] and ORB-SLAM [31]. We also assess keyframe-based offline SfM systems including ENFT-SfM [44] and VisualSfM [41] in our comparison for a comprehensive evaluation. The methods are tested on TUM-RGBD [14] and KITTI Odometry [13] datasets. For all the sequences on both datasets we use SIFT [28] features for feature matching followed by RANSAC [11] iterations to remove feature correspondence outliers, we have implemented and modified Ceres Solver [1] for local BA, and followed the algorithm in [30] for the global alignment.

5.2. Evaluations on Real-World Data

Evaluation on TUM RGB-D. As a challenging dataset for monocular online systems, the TUM RGB-D dataset contains specific RGB-D sequences including rotation-only motion and textureless surface scanning in a small scene, captured by Kinect. As we do not rely on depth information in our system, we run experiments on a selected part of the dataset which are suitable for monocular systems and evaluate the results of camera trajectory against state-of-the-art systems. The quantitative comparison results can be found in Table 1. Note that DVO-SLAM, Kintinuous and Elastic Fusion use the depth data in their experiments, ENFT-SfM and VisualSfM are mostly processed offline. We quote the experiment results of VisualSfM from [44], where the authors state that the results are achieved from their manually-extracted keyframes off-line. Though our approach achieves clear outperformances on most of the sequence, ORB-SLAM shows strong robustness dealing with dynamic objects (in *fr2_desk* sequence).

Evaluation on KITTI Odometry. The KITTI dataset contains 11 video sequences captured by a fast-moving vehicle over long camera trajectories. In the experiments it has been shown that systems like ORB-SLAM which has a

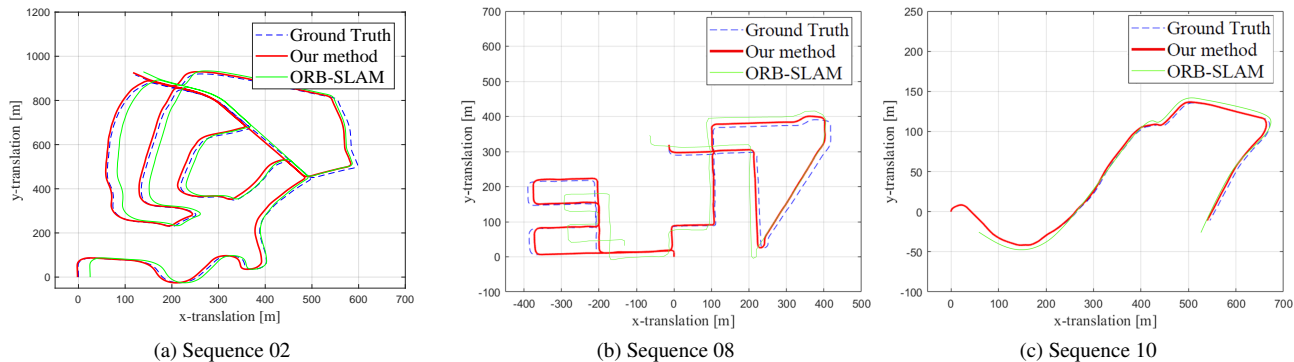


Figure 5: Comparison with ORB-SLAM on Seq.02, 08, 10 from KITTI Odometry. Our proposed approach shows a trajectory estimation of comparably high quality in large scale outdoor scenes. Note on Seq.02 it is clearly shown that ORB-SLAM (in green) suffers from accumulated drifts although the trajectory contains many loops. Results on the rest of the dataset are provided in the supplementary materials where our approach outperforms ORB-SLAM on all of the sequences.

heavy reliance on explicit loop closures suffer on several sequences from the dataset. Since our proposed approach ensures global consistency by consecutively aligning the partitions rather than loose-connected keyframes, it convincingly shows the robustness on large-scale outdoor scenes.

Seq	ENFT SFM [44]	Vis. SFM [41]	ORB SLAM [31]	OURS
00	4.8	2.8 /3.7%	5.3 /24.83s	2.5 /5.65s
01	57.2	52.3 /12.5%	-	37.4 /14.96s
02	28.3	1.8 /4.5%	21.3 /30.07s	15.1 /7.26s
03	2.9	0.3 /12.0%	1.5 /4.88s	1.2 /0.93s
04	0.7	0.8 /23.4%	1.6 /1.58s	0.3 /0.17s
05	3.5	9.8 /7.4%	2.9 /15.20s	2.8 /2.35s
06	14.4	8.6 /7.4%	12.3 /7.78s	6.3 /0.84s
07	2.0	3.9 /7.8%	2.3 /6.28s	2.0 /0.91s
08	28.3	0.8 /0.9%	46.7 /25.60s	19.7 /15.87s
09	5.9	0.9 /4.9%	6.6 /11.33s	6.2 /2.54s
10	18.5	5.7 /6.5%	8.8 /7.64s	5.2 /1.02s

Table 2: Trajectory estimation RMSE(m) and pose estimation runtime on KITTI Odometry. For VisualSfM the second number represents the map completeness ratio and it is 100% for all other methods. For ORB-SLAM the second number represents the BA runtime and our pose estimation is around 10x faster on several sequences. We achieve superior results on almost all of the sequences except on Seq.09 where ENFT-SfM performs slightly better. Note that ENFT-SfM and VisualSfM are offline SfM systems and the latter requires preprocessings. ORB-SLAM fails to initialize on Seq.01 so we leave the result blank.

Quantitative Comparison The quantitative comparisons of our estimations against ENFT-SfM, VisualSfM and ORB-SLAM are shown in Table. 2. We quote the results of VisualSfM from [44], where the authors pointed out that the trajectories are overly long for VisualSfM, resulting in disconnected blocks of trajectories. Hence the RMSE results are calculated by taking the largest component of the

trajectory. For example, on Seq.02 the RMSE is computed based on 4.5% of the whole trajectory. Moreover, ORB-SLAM fails to process Seq.01 due to lost of tracking at the beginning of the video sequence.

Qualitative Comparison Though ORB-SLAM is able to correctly detect and close the loop in Seq.02, it still shows a clear drift compared with our approach, our approach also shows a clearly more accurate estimation on Seq.08 and Seq.10 (in Fig. 5). Seq.08 does not contain loops so ORB-SLAM suffers from serious drifts both on translations and scale. While on Seq.10 ORB-SLAM has lost tracking from the beginning of the sequence and also shows accumulated drifts by the end of trajectory estimation. The rest of the qualitative comparisons are given in the supplementary materials, where our approach outperforms ORB-SLAM on all of the sequences.

6. Conclusion

In this paper, we propose a hybrid formulation with on-line partitioning to solve the real-time camera pose estimation problem in a quasi-distributed manner. Our partitioning scheme effectively ensures the strong connectivity between the cameras and the blocks, such that the pose estimation accuracy is significantly improved. With the propagation of intermediate computation values, our proposed self-adaptive Levenberg-Marquardt solver of a proven quadratic convergence rate further enhances the efficiency of local BA. The inter-block dense data association enables us to introduce single rotation averaging for the global alignment, as to avoid the high computational costs and explicit loop closings in conventional global BA frameworks. Clear outperformances against state-of-the-art monocular systems with conventional BA further demonstrate the practicality and robustness of our proposed approach.

References

- [1] S. Agarwal, K. Mierle, and Others. Ceres solver. <http://ceres-solver.org>. 7
- [2] A. P. Bustos, T.-J. Chin, A. Eriksson, and I. Reid. Visual slam: Why bundle adjustment. In *Proceedings - IEEE International Conference on Robotics and Automation (ICRA)*, 2019. 1, 2
- [3] A. Chatterjee and V. M. Govindu. Robust relative rotation averaging. *IEEE transactions on pattern analysis and machine intelligence*, 40(4):958–972, 2018. 1
- [4] A. Chatterjee and V. Madhav Govindu. Efficient and robust large-scale rotation averaging. In *Proceedings of the IEEE International Conference on Computer Vision*, pages 521–528, 2013. 1
- [5] H. Cui, X. Gao, S. Shen, and Z. Hu. Hsfm: Hybrid structure-from-motion. In *Proceedings of the IEEE Conference on Computer Vision and Pattern Recognition*, pages 1212–1221, 2017. 1, 2
- [6] H. Cui, S. Shen, X. Gao, and Z. Hu. Csfm: community-based structure from motion. In *2017 IEEE International Conference on Image Processing (ICIP)*, pages 4517–4521. IEEE, 2017. 1
- [7] Z. Cui and P. Tan. Global structure-from-motion by similarity averaging. In *Proceedings of the IEEE International Conference on Computer Vision*, pages 864–872, 2015. 1
- [8] A. Eriksson, J. Bastian, T.-J. Chin, and M. Isaksson. A consensus-based framework for distributed bundle adjustment. In *Proceedings of the IEEE Conference on Computer Vision and Pattern Recognition*, pages 1754–1762, 2016. 1
- [9] J. Fan and J. Pan. Convergence properties of a self-adaptive levenberg-marquardt algorithm under local error bound condition. *Computational Optimization and Applications*, 34(1):47–62, 2006. 6, 7
- [10] J.-y. Fan and Y.-x. Yuan. On the quadratic convergence of the levenberg-marquardt method without nonsingularity assumption. *Computing*, 74(1):23–39, 2005. 7
- [11] M. A. Fischler and R. C. Bolles. Random sample consensus: a paradigm for model fitting with applications to image analysis and automated cartography. *Communications of the ACM*, 24(6):381–395, 1981. 7
- [12] J. Fredriksson and C. Olsson. Simultaneous multiple rotation averaging using lagrangian duality. In *Asian Conference on Computer Vision*, pages 245–258. Springer, 2012. 1
- [13] A. Geiger, P. Lenz, C. Stiller, and R. Urtasun. Vision meets robotics: The KITTI dataset. *International Journal of Robotics Research*, 2013. 6, 7
- [14] A. Handa, T. Whelan, J. McDonald, and A. J. Davison. A benchmark for RGB-D visual odometry, 3D reconstruction and SLAM. In *Proceedings - IEEE International Conference on Robotics and Automation*, 2014. 7
- [15] R. Hartley, J. Trumpf, Y. Dai, and H. Li. Rotation averaging. *International journal of computer vision*, 103(3):267–305, 2013. 1
- [16] M. Havlena, A. Torii, and T. Pajdla. Efficient structure from motion by graph optimization. In *European Conference on Computer Vision*, pages 100–113. Springer, 2010. 1
- [17] L. Hei. A self-adaptive trust region algorithm. *Journal of Computational Mathematics*, pages 229–236, 2003. 6
- [18] V. Ila, L. Polok, M. Solony, and P. Svoboda. Slam++-a highly efficient and temporally scalable incremental slam framework. *The International Journal of Robotics Research*, 36(2):210–230, 2017. 1
- [19] V. Indelman, R. Roberts, C. Beall, and F. Dellaert. Incremental Light Bundle Adjustment. In *Proceedings of the British Machine Vision Conference*, 2012. 1
- [20] M. Kaess, A. Ranganathan, and F. Dellaert. isam: Incremental smoothing and mapping. *IEEE Transactions on Robotics*, 24(6):1365–1378, 2008. 1
- [21] C. Kanzow, N. Yamashita, and M. Fukushima. Levenberg-Marquardt methods with strong local convergence properties for solving nonlinear equations with convex constraints. *Journal of Computational and Applied Mathematics*, 2005. 7
- [22] C. Kerl, J. Sturm, and D. Cremers. Dense visual SLAM for RGB-D cameras. In *IEEE International Conference on Intelligent Robots and Systems*, 2013. 7
- [23] K. Konolige and M. Agrawal. FrameSLAM: From bundle adjustment to real-time visual mapping. *IEEE Transactions on Robotics*, 2008. 1
- [24] J. B. Kruskal. On the shortest spanning subtree of a graph and the traveling salesman problem. *Proceedings of the American Mathematical society*, 7(1):48–50, 1956. 4
- [25] K. Levenberg. A method for the solution of certain nonlinear problems in least squares. *Quarterly of Applied Mathematics*, 1944. 4
- [26] H. Liu, M. Chen, G. Zhang, H. Bao, and Y. Bao. ICE-BA: Incremental, Consistent and Efficient Bundle Adjustment for Visual-Inertial SLAM. *cvpr*, 2018. 1
- [27] A. Locher, M. Havlena, and L. V. Gool. Progressive structure from motion. In *Proceedings of the IEEE European Conference on Computer Vision (ECCV)*, 2018. 1, 2
- [28] D. G. Lowe. Distinctive image features from scale-invariant keypoints. *International Journal of Computer Vision*, 2004. 7
- [29] R. Maier, J. Sturm, and D. Cremers. Submap-based bundle adjustment for 3D reconstruction from RGB-D data. In *Lecture Notes in Computer Science (including subseries Lecture Notes in Artificial Intelligence and Lecture Notes in Bioinformatics)*, 2014. 1
- [30] J. H. Manton. A globally convergent numerical algorithm for computing the centre of mass on compact lie groups. In *ICARCV 2004 8th Control, Automation, Robotics and Vision Conference, 2004.*, volume 3, pages 2211–2216. IEEE, 2004. 5, 7
- [31] R. Mur-Artal, J. M. Montiel, and J. D. Tardos. ORB-SLAM: A Versatile and Accurate Monocular SLAM System. *IEEE Transactions on Robotics*, 2015. 7, 8
- [32] K. Ni, D. Steedly, and F. Dellaert. Out-of-core bundle adjustment for large-scale 3D reconstruction. In *Proceedings of the IEEE International Conference on Computer Vision*, 2007. 1
- [33] S. Pettie and V. Ramachandran. A randomized time-work optimal parallel algorithm for finding a minimum spanning for-

- est. *SIAM Journal on Computing*, 31(6):1879–1895, 2002. 5
- [34] J. L. Schonberger and J.-M. Frahm. Structure-from-motion revisited. In *Proceedings of the IEEE Conference on Computer Vision and Pattern Recognition*, pages 4104–4113, 2016. 1
- [35] H. Shum, Q. Ke, and Z. Zhang. Efficient bundle adjustment with virtual key frames: a hierarchical approach to multi-frame structure from motion. In *Conference on Computer Vision and Pattern Recognition (CVPR)*, 1999. 1
- [36] D. Sibley and C. Mei. Adaptive relative bundle adjustment. In *Robotics: science and systems*, 2009. 1
- [37] D. Steedly, I. Essa, and F. Dellaert. Spectral partitioning for structure from motion. Georgia Institute of Technology, 2003. 1
- [38] M. Vo, S. G. Narasimhan, and Y. Sheikh. Spatiotemporal Bundle Adjustment for Dynamic 3D Reconstruction. In *2016 IEEE Conference on Computer Vision and Pattern Recognition (CVPR)*, 2016. 1
- [39] T. Whelan, M. Kaess, M. Fallon, H. Johannsson, J. Leonard, and J. McDonald. Kintinuous: Spatially Extended Kinect-Fusion. *Computer Science and Artificial Intelligence Laboratory Technical Report*, 2012. 7
- [40] T. Whelan, S. Leutenegger, R. Salas Moreno, B. Glocker, and A. Davison. ElasticFusion: Dense SLAM Without A Pose Graph. In *Robotics: Science and Systems XI*, 2015. 7
- [41] C. Wu. Visualsfm: A visual structure from motion system. 2011. 7, 8
- [42] C. Wu. Towards linear-time incremental structure from motion. In *Proceedings - 2013 International Conference on 3D Vision, 3DV*, 2013. 1
- [43] N. Yamashita and M. Fukushima. On the rate of convergence of the levenberg-marquardt method. In *Topics in numerical analysis*, pages 239–249. Springer, 2001. 6
- [44] G. Zhang, H. Liu, Z. Dong, J. Jia, T. T. Wong, and H. Bao. Efficient Non-Consecutive Feature Tracking for Robust Structure-From-Motion. *IEEE Transactions on Image Processing*, 2016. 7, 8
- [45] R. Zhang, S. Zhu, T. Fang, and L. Quan. Distributed very large scale bundle adjustment by global camera consensus. In *Proceedings of the IEEE International Conference on Computer Vision*, pages 29–38, 2017. 1
- [46] S. Zhu, T. Shen, L. Zhou, R. Zhang, J. Wang, T. Fang, and L. Quan. Parallel structure from motion from local increment to global averaging. *arXiv preprint arXiv:1702.08601*, 2017. 1
- [47] S. Zhu, R. Zhang, L. Zhou, T. Shen, T. Fang, P. Tan, and L. Quan. Very large-scale global sfm by distributed motion averaging. In *Proceedings of the IEEE Conference on Computer Vision and Pattern Recognition*, pages 4568–4577, 2018. 1